archives
of thermodynamics
Vol. **40**(2019), No. 2, 3–16
DOI: 10.24425/ather.2019.129539

Numerical simulation of forced convection of nanofluid around a circular cylinder

KAMEL KORIB[a]
NABILA IHADDADENE[b]
RAFIK BOUAKKAZ[c*]
YACINE KHELILI[a]

[a] Department of Mechanical Engineering, University Saad Dahlab, Blida, Algeria

[b] Département de génie mécanique Pôle universitaire de M'Sila, M'Sila 28000 Algeria

[c] Military Academy of Cherchell,Tipaza, Algeria

Abstract In this study a steady flow-field and heat transfer through a copper-water nanofluid around a circular cylinder, under the influence of both the standard thermal boundary conditions, i.e., uniform heat flux and constant wall temperature) was investigated numerically by using a finite-volume method for Reynolds numbers from the range 10–40. Furthermore, the range of nanoparticle volume fractions considered is 0–5%. The variation of the local and the average Nusselt numbers with Reynolds number, and volume fractions are presented for the range of conditions. The average Nusselt number is found to increase with increasing the nanoparticle volume fractions.

Keywords: Copper nanoparticles; Heat transfer; Circular cylinder; Steady regime

Nomenclature

c_p	–	heat capacity, J/(kg K)
D_t	–	diameter of the cylinder, m

*Corresponding Author. Email: r.boukkaz@gmail.com

k – thermal conductivity, W/(m K)
L – lift force, N
Nu – local Nusselt number
$\overline{\mathrm{Nu}}$ – average Nusselt number
Nu_0 – average Nusselt number for the stationary cylinder
P – local pressure, N/m^2
Re – Reynolds number,
Pr – Prandtl number
T_∞ – free-surface temperature
U_∞ – free-stream velocity,m/s
u – stream-wise velocity, m/s
v – cross-stream velocity, m/s

Greek symbols

α – non-dimensional rotation rate
φ – nanoparticle volume fractions
ϕ – angular displacement from the front stagnation point
θ – non-dimensional temperature
ν – kinematic viscosity, m^2/s
ρ – density, kg/m^3

Subscripts

f – base fluid
nf – nanofluid
s – solid nanoparticular

1 Introduction

In recent years, fluid flow and heat transfer around cylinders has been a subject of great interest for researchers due to its high applicability in many industrial developments. The authors of the work [1] using standard boundary conditions namely constant wall temperature (CWT) studied the local and average heat transfer characteristics around a circular cylinder for the Reynolds number range of 2×10^3–9×10^4 and Prandtl number range 0.7–176. Three regions of flow: laminar boundary layer, reattachment of shear layer and periodic vortex regions were indicated around the cylinder for sub-critical flow. Further, they developed an empirical correlation for predicting the overall heat transfer from these three regions. Also, the authors [2] using uniform dissipating heat flux boundary conditions (UHF) investigated numerically the free stream flow and forced convection heat transfer across a rotating cylinder for Reynolds numbers of Re = 10–45 and $0.7 < \mathrm{Pr} < 400$. Their results show that the heat transfer is increasing with increase in Re and/or Pr numbers.

The flow and heat transfer across the isothermal rotating cylinder with the rate of rotation in the range $0 \leq \alpha \leq 6$ and Reynolds number varying from 20–160 was carried by [3–5]. In the depth analysis, they revealed that the rotation can be used as a drag reduction and heat transfer suppression technique. Further, [6] studied were numerically the free stream flow and forced convection heat transfer across a rotating cylinder, dissipating heat flux for Reynolds numbers of 20–160 and a Prandtl number of 0.7. Their results show that at higher rotational velocity, the Nusselt number is almost independent of Reynolds number as well as the thermal boundary conditions.

In past studies, the fluids used have a low value of thermal conductivity, which limits the heat transfer. For this reason, there are several methods to improve the heat transfer characteristics, which consist in adding high conducting solid particles in to the base fluid. The resulting fluid is called the 'nanofluid' [6–8]. The steady flow-field and heat transfer through a copper-water nanofluid around circular cylinder was numerically simulated by [9]. The values of vorticity, pressure coefficient, recirculation length are increased by the addition of nanoparticles into the base fluid. Subsequently, [10] examined were the effect of heat treatment process with a new cooling medium (nanofluid), which contains water with Cu, Ag or Al_2O_3 particles, on heat transfer characteristics and mechanical properties of the unsteady continuous moving cylinder in the thermal forces. They reported that the Al_2O_3 nanofluid is the best type of nanofluid for improving the mechanical properties of the surface (increase of the heat flux). This nanofluid is also the best type for decreasing the surface shear stress. Recently in [11] authors have focused on A numerical study of heat transfer phenomena over an isothermal cylinder, for low Reynolds number flow of nanofluid. Heat transfer characteristic and flow over the stationary cylinder has been studied for water based copper nanofluid with different solid fraction values. They have shown that the presence of nanoparticle has no effect on the point of flow separation for a fixed Reynolds number because the effect of buoyancy force has not been taken into consideration.

On the other hand in [12] have been studied the momentum and forced convection heat transfer for a laminar and steady free stream flow of nanofluids past a square cylinder. Different nanofluids consisting of Al_2O_3 and CuO with base fluids of water and a 60:40 (by mass) ethylene glycol and water mixture were selected to evaluate their superiority over conventional fluids. They showed that for any given particle diameter there is an optimum

value of particle concentration that results in the highest heat transfer coefficient. The fluid flow and heat transfer around a square cylinder utilizing Al_2O_3-H_2O nanofluid over low Reynolds numbers varied within the range from 1 to 40 and the volume fraction of nanoparticles (φ) varied within the range from $0 < \varphi < 0.05$ was investigated by [13]. They found that the increasing of the nanoparticles volume fractions augments the drag coefficient. Moreover, pressure coefficient increases by increasing the solid volume fraction for sides where pressure gradient is inverse but for sides where the pressure gradient is favourable the pressure coefficient decreases. The present investigation had been motivated by increased interest and research in potential improvements in the heat transfer characteristics using nanofluids. Effort has been made to investigate numerically the steady flow of nanofluid and heat transfer characteristics under the influence of both the standard thermal for a range of Reynolds numbers 10–40 and particle volumetric concentrations ranging from 0% to 5%.

2 Problem statement, governing equations, and boundary conditions

The system here consists of a 2D infinitely long circular cylinder having a diameter D_t. It is exposed to a constant free stream velocity of U_∞ at a uniform temperature of T_∞ at the inlet. The nanoparticles are assumed to be uniform shape and size. In addition, we have assumed that nanoparticles are in thermal equilibrium state and flowing at the same velocity. Flow configuration is shown in Fig. 1.

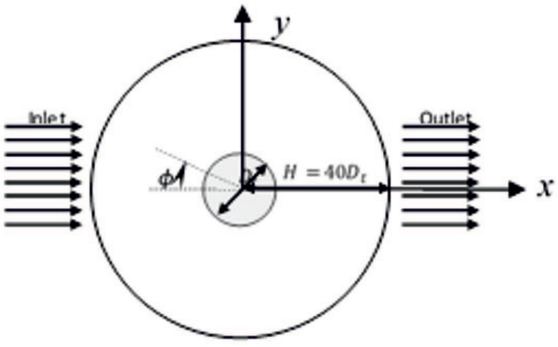

Figure 1: Schematic of the unconfined flow past a cylinder.

2.1 Governing equations and boundary conditions

The governing partial differential equations here are the Navier-Stokes and energy equations in two dimensions and steady state nanofluid flow around a circular cylinder are:

$$\frac{\partial U}{\partial X} + \frac{\partial V}{\partial Y} = 0\,, \tag{1}$$

$$U\frac{\partial U}{\partial X} + V\frac{\partial U}{\partial Y} = -\frac{\partial P}{\partial X} + \frac{1}{\mathrm{Re}}\frac{v_{nf}}{v_f}\left(\frac{\partial^2 U}{\partial X^2} + \frac{\partial^2 U}{\partial Y^2}\right)\,, \tag{2}$$

$$U\frac{\partial V}{\partial X} + V\frac{\partial V}{\partial Y} = -\frac{\partial P}{\partial Y} + \frac{1}{\mathrm{Re}}\frac{v_{nf}}{v_f}\left(\frac{\partial^2 V}{\partial X^2} + \frac{\partial^2 V}{\partial Y^2}\right)\,, \tag{3}$$

$$U\frac{\partial \theta}{\partial X} + V\frac{\partial \theta}{\partial Y} = \frac{1}{\mathrm{RePr}}\frac{\alpha_{nf}}{\alpha_f}\left(\frac{\partial^2 \theta}{\partial X^2} + \frac{\partial^2 \theta}{\partial Y^2}\right)\,, \tag{4}$$

where

$$U = \frac{u}{U_\infty}\,,\ V = \frac{v}{U_\infty}\,,\ X = \frac{x}{D_t}\,,\ Y = \frac{y}{D_t}\,,\ P = \frac{p}{\rho_{nf}U_\infty^2}\,,$$

$$\mathrm{Pr} = \frac{v_f}{\alpha_f},\ \mathrm{Re} = \frac{U_\infty D_t}{v_f}\,,\ \theta = \frac{T-T_\infty}{T_W-T_\infty}\,.$$

Here U and V are the velocity components along X- and Y-axes, θ denote the temperature, P the pressure, ρ the density, and ν the kinematic viscosity, respectively. Pr and Re are the Prandtl and Reynolds numbers, respectively, α is the rotation rate. The subscript nf stands for nanofluid, the subscript f stands for base fluid and the subscript s stands for solid nanoparticles. The capital letters represent dimensionless values.

The thermophysical properties taken from [9], for the base fluid and the copper oxide (at 300 K) are shown in Tab. 1.

Table 1: Thermophysical properties of the base fluid and the Cu nanoparticles.

Property	unit	water	copper
heat capacity, C_p	$\mathrm{J\,Kg^{-1}K^{-1}}$	4179	385
density, ρ	$\mathrm{kg\,m^{-3}}$	997.1	8.933
thermal conductivity, k	$\mathrm{W\,m^{-1}K^{-1}}$	0.613	401

The effective density, thermal diffusivity, heat capacitance, effective dynamic viscosity and the effective thermal conductivity of the nanofluid are calculated using the following expressions:

$$\rho_{nf} = (1-\varphi)\,\rho_f + \varphi\rho_s\,, \tag{5}$$

$$(\rho C_p)_{nf} = (1-\varphi)\,(\rho C_p)_f + \varphi\,(\rho C_p)_s\,, \tag{6}$$

$$\alpha_{nf} = k_{nf}/\,(\rho C_p)_{nf}\,, \tag{7}$$

$$\mu_{nf} = \frac{\mu_f}{(1-\varphi)^{2.5}}\,, \tag{8}$$

$$k_{nf} = k_{bf}\left[\frac{(k_s+2k_f)-2\varphi\,(k_f-k_s)}{(k_s+2k_f)+\varphi\,(k_f-k_s)}\right]\,, \tag{9}$$

where φ is the solid volume fraction.

2.2 Boundary conditions

The dimensionless boundary conditions for the flow across a circular cylinder can be written as (Fig.1). The left-hand arc is the inflow section or upstream section, where there is the Dirichlet-type boundary condition for the Cartesian velocity components

$$U = V = 0 \quad \theta = 0\,, \tag{10}$$

The right-hand arc represents the outflow boundary, where it is considered that the diffusion flux in the direction normal to the exit surface is zero for all variables

$$\frac{\partial U}{\partial X} = \frac{\partial V}{\partial X} = \frac{\partial \theta}{\partial X} = 0. \tag{11}$$

Finally, the dimensionless peripheral or tangential velocity is prescribed on the surface of the cylinder,along with a no-slip boundary condition:

$$\begin{aligned} U = 0, \quad V = 0, \quad \frac{\partial \theta}{\partial X} = -1 \quad \text{for} \quad \text{UHF;} \\ U = 0, \quad V = 0, \quad \theta = 1 \quad \text{for} \quad \text{CWT.} \end{aligned} \tag{12}$$

Here, in case of CWT, non-dimensional temperature is given as $\theta = \frac{T-T_\infty}{T_W-T_\infty}$ while for UHF, the non-dimensional temperature is given as $\theta = \frac{T-T_\infty}{(q_w D/k)}$, where n_s is the normal unit direction vector away from the cylinder surface.

3 Numerical details

The steady, laminar, segregated solver was employed here to solve the incompressible flow on the collocated grid arrangement. Semi implicit method for the pressure linked equations (SIMPLE) was used to solve Navier-Stokes and energy equations for above noted boundary conditions. Second order upwind scheme is used to discretize the convective terms of momentum equations, whereas the diffusive terms are discretized by central difference method. A convergence criterion of 10^{-8} is used for continuity, and x-, y-components of momentum equations. While, for energy equation the criteria of convergence was 10^{-10}.

Table 2: Effect of grid number on averaged Nusselt number at Re = 40, Pr = 4.76 ($\varphi = 0.05$).

Mesh	Cells	N_t	h_{Dt}/D_t	$\overline{\mathrm{Nu}}$
M1	32000	160	0.0015	9.3447
M2	40000	200	0.0010	9.3766
M4	50000	250	0.0010	9.3688

3.1 Domain independence study

The mesh used for all the two-dimensional computations consisted of 40000 quadrilateral cells and 40200 nodes. The cylinder (of diameter D_t) resides in a computational domain whose outer edges located at a distance of H from the center of the cylinder (Fig. 1). There are N_t points in the circumferential direction on the cylinder surface and the radial thickness of the first layer of cells (i.e., cells attached to the wall) is h_{Dt}. In this study, following authors [3,4], the computational domain extends 40 times the diameter of the cylinder in all directions. The grids sensitivity analysis is performed for Re = 40 and $\varphi = 0.05$. Table 2 lists the details for the meshes that were employed. As regarding the influence of the number of grid points on the average Nusselt number on the wall of cylinder, it was decided to carry out the computations in this work with mesh M2.

4 Results and discussion

4.1 Comparison with other results

The first step was to validate the problem set-up. The choice of numerical methods and mesh attributes was accomplished by comparing results from our numerical simulations with results obtained from the literature. The outcomes included in the comparison were the mean Nusselt number.

Table 3: Comparison of Nu number computed in the present study with literature data (Pr = 0.7).

Boundary conditions	Re	Nu		Relative error (%)
		Paramane *et al.* [4]	Present study	
UHF	20	2.7499	2.7382	0.43
	40	3.7499	3.7618	0.32
CWT		Paramane *et al.* [6]		
	20	2.4092	2.4189	0.40
	40	3.2496	3.2465	0.10

4.2 Streamlines pattern

The streamlines around cylinder are compared between base fluid and nanofluid ($\varphi = 0.05$) in Fig. 2 at Reynolds number ranging from 20 to 40 at UHF boundary conditions. For high Reynolds number the recirculation bubble becomes big and strong at the downstream side of the cylinder for both base fluid and nanofluid. However, in nanofluid the center of bubbles is slightly pushed away from the surface of the cylinder comparing with the base fluid.

4.3 Isotherm patterns

The isotherms profiles around the cylinder for Reynolds number of 40 for UHF boundary conditions are compared between base fluid and nanofluid ($\varphi = 0.05$) in Fig. 3. Clearly, the temperature distribution contours for base fluid are overlaid with that for nanofluid. This can be explained as the

addition of solid particles to the base fluid increases the Reynolds number of nanofluid. Hence, the higher capacity of transferring the heat from the cylinder. It is obvious from Fig. 3 that the isotherms have a maximum density close to the front surface of the cylinder; this indicates high values of the local Nusselt number near the front stagnation point on the front surface as compared to other points on the cylinder surface.

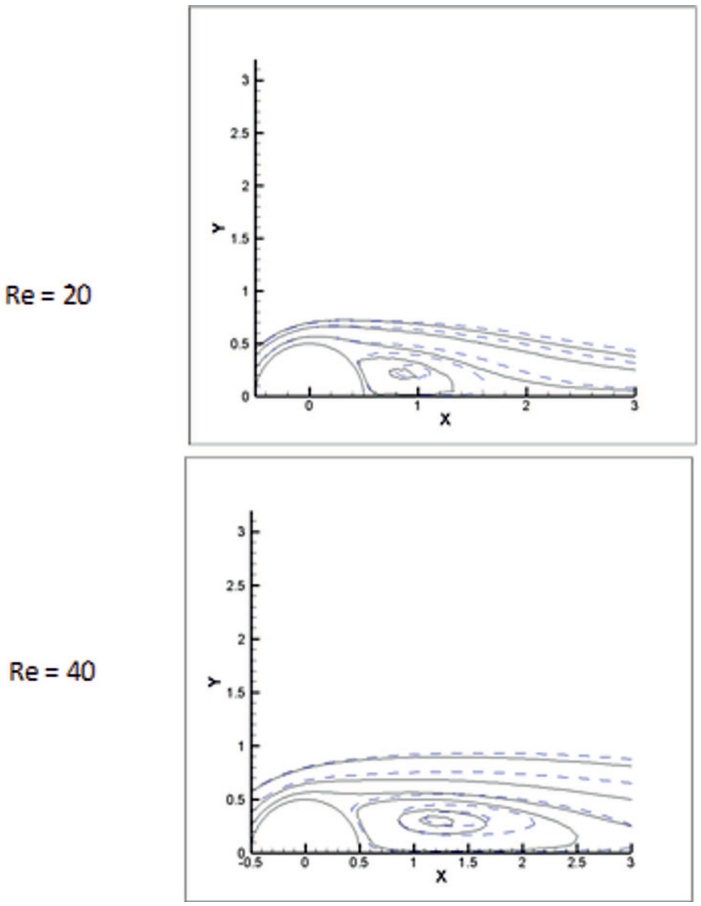

Figure 2: Streamlines contours for the flow around the cylinder (solid line refers to base fluid and dashed line refers to nanofluid with solid volume fraction 0.05) for UHF boundary conditions.

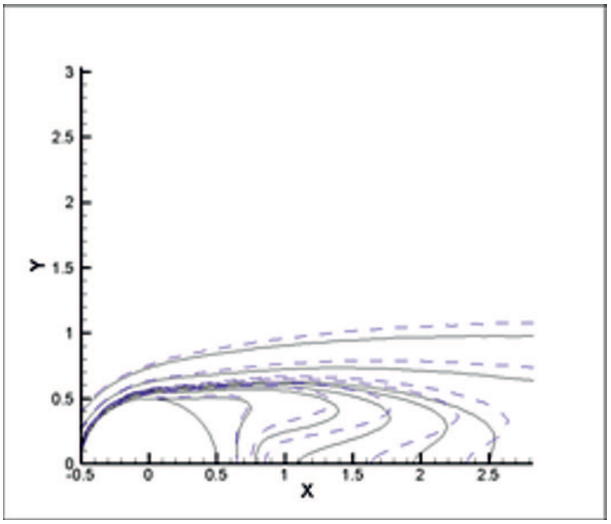

Figure 3: Temperature contours for the flow around the cylinder (solid line refers to base fluid and dashed line refers to nanofluid with solid volume fraction 0.05) for UHF boundary conditions at Re = 40.

4.4 Local Nusselt number

Figure 4 shows the variation of local Nusselt number (Nu) on the surface of the cylinder with increase in Reynolds number (Re) for various volume fraction (φ). When the solid concentration increases the thermal conductivity improves and consequently the local Nusselt number. Additionally, the thermal boundary layer is decreased by any increase in solid volume fraction. Therefore, the local Nusselt number is enhanced by any increasing in solid volume fraction.

On the other hand, for all Re, the variation of Nusselt number found to be symmetrical at $\phi = 90°$. The value of the local Nu number is maximum on the front ($\phi = 0$) and minimum on the rear ($\phi = 180°$) side of the cylinder. Also, at Re = 40, a kink is observed in the values of local Nusselt number. It can be explained on the basis that higher Reynolds number results in lager recirculation region. Also, Tab. 4 presents the difference due to adding solid nanoparticles fraction in Nu. As expected, the table shows that the values of Nu_{max} or Nu_{min} are greater for UHF boundary condition.

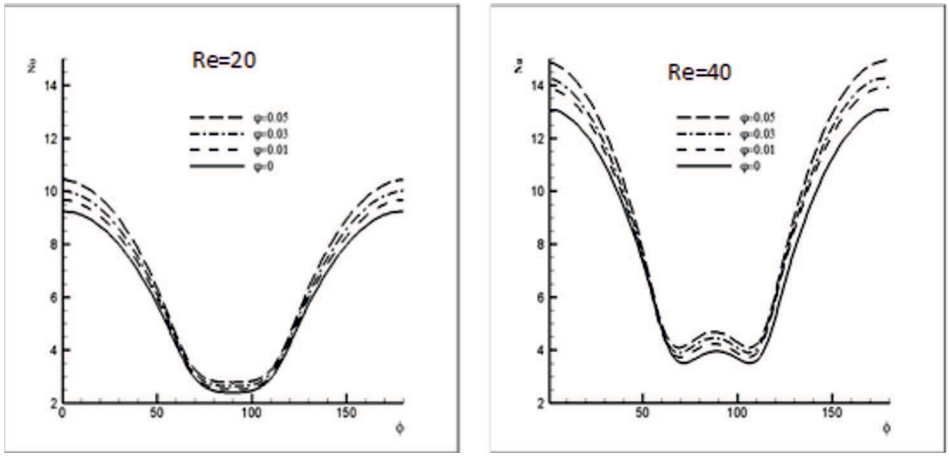

Figure 4: Local Nusselt number variation at various solid volume fractions for varying values of Reynolds number and rotation rate, UHF boundary conditions.

Table 4: Comparison of Nu number computed in the present study with literature data (Pr = 0.7).

φ	Nu_{max}			Nu_{min}		
	UHF	CWT	Difference (UHF-CWT)	UHF	CWT	Difference (UHF-CWT)
0.01	13.9325	13.4567	0.4758	3.72545	2.51057	1.21488
0.03	14.2648	14.1116	0.1532	3.89675	2.63901	1.25774
0.05	14.9385	14.7632	0.1753	4.09028	2.07218	2.0181

4.5 Averaged Nusselt number

The average Nusselt number variation is presented in Fig. 5 for the solid volume fraction varying from 0 to 0.05 in the steady regime. This figure indicates that the averaged Nusselt number increases linearly with increasing solid volume fraction of nanoparticles (φ) at different Reynolds numbers. This can be explained as when the Re number increases the inertia of flow increases thus increasing the heat transfer. The effect of Reynolds number also increases with increase in volume fraction number, the Reynolds and

Prandtl number of nanofluids can be expressed as

$$\mathrm{Re}_{nf} = \frac{\rho_{nf}}{\rho_f}\frac{\mu_f}{\mu_{nf}}\,\mathrm{Re}\,, \qquad \mathrm{Pr}_{nf} = \frac{\mu_{nf}}{\mu_f}\frac{C_{P,nf}}{C_{P,f}}\frac{k_f}{k_{nf}}\,\mathrm{Pr}\,.$$

Further, the UHF boundary condition yields higher values of the average Nusselt number.

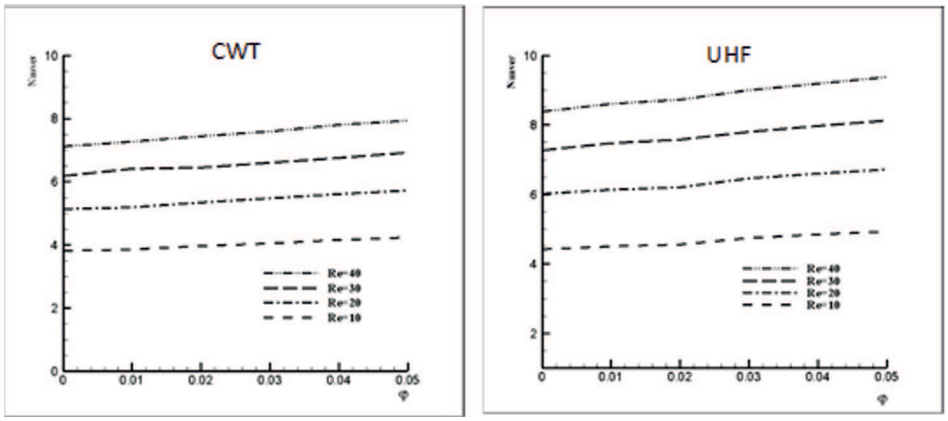

Figure 5: Variation of average Nusselt number at various solid volume fractions for varying values of Reynolds number.

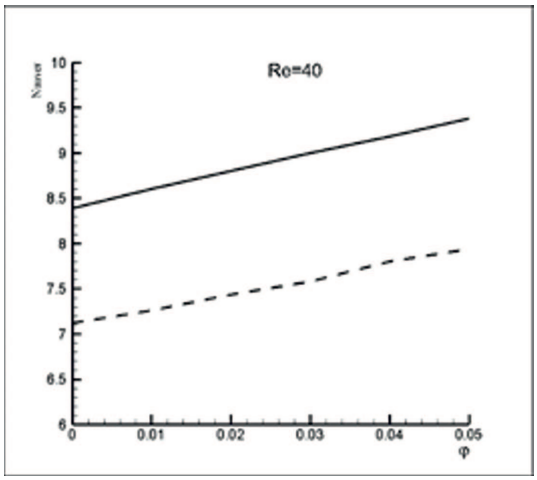

Figure 6: Average Nusselt number variation for $(0 \leq \varphi \leq 5)$ at UHF (solid lines) and CWT (dashed lines).

5 Conclusions

The present study focuses on the unconfined laminar flow of nanofluid and heat transfer characteristics around a circular cylinder under the influence of both the thermal boundary conditions, i.e., UHF and CWT in the steady regime. The illustrative streamline patterns and isotherm patterns are presented and examined for the above range of conditions. It was showed that at a given Reynolds number, local and average Nusselt numbers were enhanced by adding nanoparticles to base fluid. Moreover, the UHF boundary condition yields higher values of the average Nusselt number.

Received in 31 March 2017

References

[1] Sanitjai S., Goldstein R.J.: *Forced convection heat transfer from a circular cylinder in crossflow to air and liquids*. Int. J. Heat Mass Tran. **47**(2004), 22, 4795–4805

[2] Bharti R.P., Chhabra R.P., Eswaran V.: *A numerical study of the steady forced convection heat transfer from an unconfined circular cylinder*. Heat Mass Tran. **43**(2007), 7, 639–648.

[3] Sufyan M., Manzoor S., Sheikh N.A.: *Heat transfer suppression in flow around a rotating circular cylinder at high Prandtl number*. Arab. J. Sci. Eng. **39**(2014), 11, 8051–8063.

[4] Paramane S.B., Sharma A.: *Numerical investigation of heat and fluid flow across a rotating circular cylinder maintained at constant temperature in 2D laminar flow regime*. Int. J. Heat Mass Tran. **52**(2009), 13-14, 3205–3216.

[5] Bouakkaz R., Talbi K., Khelil Y., SalhiF., Belghar N., Ouazizi M.: *Numerical investigation of incompressible fluid flow and heat transfer around a rotating circular cylinder*. Thermophys. Aeromech. **21**(2014), 1, 87–97.

[6] Paramane S.B., Sharma A.: *Heat and fluid flow across a rotating cylinder dissipating uniform heat flux in 2D laminar flow regime*. Int. J. Heat Mass Tran. **53**(2010), 21–22, 4672–4683.

[7] Brinkman H.C.: *The viscosity of concentrated suspensions and solutions*. J. Chem. Physics **20**(1952), 571–581.

[8] Rup K., Nering K.: *Unsteady natural convection in micropolar nanofluids*. Arch. Thermodyn. **35**(2014), 3, 155–170.

[9] Ho C.J., Chen M.W., Li Z.W.: *Numerical simulation of natural convection ofnanofluid in a square enclosure: effect due to uncertainties of viscosity andthermal conductivity*. Int. J. Heat Mass Tran. **51**(2008), 4506–4516.

[10] Valipour M.S., Ghadi A.Z.:*Numerical investigation of fluid flow and heat transfer around a solid circular cylinder utilizing nanofluid*. Int. Commun. Heat Mass **38**(2011), 1296–1304.

[11] El-bashbeshy E.S.M.A., Emam T.G., Abdel-Wahed M.S.: *The effect of thermal radiation, heat generation and suction/injection on the mechanical proproperties of unsteady continuous moving cylinder in a ananofluid*. Thermal Sci. **19**(2015), 5, 1591–1601.

[12] Vegad M., Satadia S.,Pradip P., Chirag P., Bhargav P.: *Heat transfer characteristics of low Reynolds number flow of nanofluid around a heated circular cylinder*. Procedia Technology **14**(2014), 348–356.

[13] Farooji V.E., Bajestan E.E.,Niazmand H.,Wongwises S.: *Unconfined laminar nanofluid flow and heat transfer around a square cylinder*. Int. J. Heat Mass Tran. **55**(2012), 1475–1485.

[14] Valipour M.S., Masoodi R., Rashidi S.,Bovand M., Mirhosseini M.: *A numerical study on convection around a square cylinder using AL2O3-H2O nanofluid*. Thermal Sci. **18**(2014), 4, 1305–1314.

[15] Yu W., Choi S.U.S.: *The role of interfacial layers in the enhanced thermal conductivity of nanofluids: A renovated Maxwell model*. J. Nanoparticle Res. **5**(2003), 167–71.

[16] Kang S., Choi H., Lee S.: *Laminar flow past a rotating circular cylinder*. Phys. Fluids **11**(1999), 11, 3312–3321.

[17] Mittal S., Kumar B.: *Flow past a rotating cylinder*. J. Fluid Mech. **476**(2003), 303–334.

[18] Padrino J.C., Joseph D.D.: *Numerical study of the steady-state uniform flow past a rotating cylinder*. J. Fluid Mech. **557**(2006), 191–223.

[19] Stojkovic D., Breuer M., Durst F.: *Effect of high rotation rates on the laminar flow around a circular cylinder*. Phys. Fluids **14**(2002), 9, 3160–3178.